

# Asymmetric Wave Propagation Through Nonlinear PT-symmetric Oligomers

J. D'Ambroise

*Department of Mathematics, Bard College, Annandale, NY 12504, USA*

P.G. Kevrekidis

*Department of Mathematics and Statistics, University of Massachusetts, Amherst, Massachusetts 01003-4515, USA*

S. Lepri

*CNR-Consiglio Nazionale delle Ricerche, Istituto dei Sistemi Complessi,  
via Madonna del piano 10, I-50019 Sesto Fiorentino, Italy*

In the present paper, we consider nonlinear PT-symmetric dimers and trimers (more generally, oligomers) embedded within a linear Schrödinger lattice. We examine the stationary states of such chains in the form of plane waves, and analytically compute their reflection and transmission coefficients through the nonlinear PT symmetric oligomer, as well as the corresponding rectification factors which clearly illustrate the asymmetry between left and right propagation in such systems. We examine not only the existence but also the dynamical stability of the plane wave states and interestingly find them to be unstable except in the vicinity of the linear limit. Lastly, we generalize our numerical considerations to the more physically relevant case of Gaussian initial wavepackets and confirm that the asymmetry in the transmission properties persists in the case of such wavepackets, as well. The role of potential asymmetries in the nonlinearity or in the gain/loss pattern is also considered.

## INTRODUCTION

Over the last fifteen years, and ever since its original proposal by Bender and co-workers [1], the study of PT-symmetric Hamiltonian systems has become a focal point for numerous investigations at the interface between theoretical physics and applied mathematics. The fundamental appeal of such systems is that they respect key physical symmetries, namely the Parity (P) and Time-reversal (T) (but not necessarily the stronger constraint of the Hamiltonian being Hermitian), thus providing an intriguing alternative set of Hamiltonians with potentially real eigenvalues. In the context that we will examine below and for standard Schrödinger Hamiltonians with a complex potential  $V$ , the above constraints of PT symmetry amount to the potential satisfying the condition  $V(x) = V^*(-x)$ .

While this field commenced as, arguably, a mathematical curiosity associated with the foundations of quantum mechanics, a number of major developments from the point of view of applications arose recently. Initially, it was realized that electromagnetic settings could provide suitable experimental systems for the realization of linear PT-symmetric Hamiltonians [2]. However, a considerable volume of developments materialized due to the work of Christodoulides and co-workers [3] who realized that nonlinear optics (and the synthetic systems that can be engineered therein) may present a fertile playground for the experimental implementation of such PT-symmetric dynamics. Furthermore, the added feature of nonlinearity typically present in such settings initiated the consideration of the effects of such PT-symmetric potentials on the nonlinear waves (such as bright or gap solitons) that may arise therein. Subsequently, the first realizations of PT-symmetry arose both in the nonlinear optics of waveguide couplers (i.e., either two waveguides with and without loss [4] – the so-called passive PT– or in the more “standard” case of one waveguide with gain and one with loss [5]) and also in that of electronic analogs thereof [6]. This progress and the perspectives that it enables towards future developments have, in turn, fueled a considerable volume of further theoretical studies. These are concerned both with the realm of models with PT-symmetric potentials in the presence of nonlinearity [7–15] and even with that of models where gain-loss contributions of a balanced form appear in front of the nonlinear term [16–18].

Another theme that has received considerable attention recently concerns the study of asymmetric (i.e., non-reciprocal) wave propagation in the context of various applications. Among the first examples discussed in the literature is the asymmetric phonon transmission through a nonlinear interface layer between two very dissimilar crystals [19]. Later on, the theoretical proposition of a thermal diode [20] induced relevant experimental realizations in [21]; similarly, an optical diode [22] was theoretically proposed [23] and experimentally realized [24]. More recently similar proposals have been presented in left-handed metamaterials [25] and have, in fact, been experimentally realized by different groups also in the context of acoustic waves in granular systems [26, 27]. In fact, recently this theme has been examined in the context of PT periodic structures which have been shown [12] to act as unidirectional invisible media (at least for sufficiently small extents of the periodic structure [28]) with transmission coefficients and phases identical to the ones in the absence of the PT-structure.

In the present work, we adopt a different perspective to that of these recent works and in fact one closer to the considerations of [29]. The latter work considered a linear lattice in the presence of a set of  $N$  (embedded within the linear lattice) nonlinear elements. It was then shown that an asymmetry within the linear or nonlinear (still

Hamiltonian though) properties of these elements would lead to an asymmetry of the relevant transmission of a plane wave through the chain. This was then extended to the more physically realistic case of a Gaussian wavepacket whose asymmetry was examined between incidence (on the asymmetric nonlinear region) from the left and from the right.

Here, we consider these notions of asymmetric wave propagation but for PT-symmetric oligomers (namely dimers, trimers, quadrimers, etc.; see also the earlier study of such oligomers [13] which has motivated further recent studies such as the examination of quadrimers in [30]). In particular, we examine both the similarities and the differences with the above picture. In particular, we start our considerations by examining the transmission of plane waves through the chain. For such states, we analytically identify their reflection and transmission coefficients and obtain the corresponding transmittivity. We find some fundamental differences here in that such a quantity may exceed unity due to the presence of gain. Furthermore, we identify another fundamental difference in that beyond a particular gain strength a supercritical amount of “mass” may be collected at the gain site that may in turn lead to indefinite growth on this site. Nevertheless, for PT-coefficient strengths which yield meaningful transmittivities, a rectification factor is computed and clearly evidences the asymmetry between left and right propagation. Another aspect of the relevant plane wave solutions that we clarify concerns their generic dynamical instability, which we quantify and illustrate the (again, focusing) dynamical manifestation thereof. Lastly, we generalize our considerations (numerically) to the prototypical physically relevant case of an incident Gaussian wavepacket. We showcase that in that case as well, the transmission result differs between left and right such wavepackets impinging on the nonlinear PT-symmetric lattice region.

It should be noted that such linear lattices with nonlinear “impurities” have been considered in the past in electronic settings (where the nonlinearity characterizes the strong interaction with local vibrations at the impurity site) [31]. They have also been examined in magnetic settings to describe tunneling through a magnetic impurity connected to two perfect leads in the presence of a magnetic field [32] and have even been generalized to higher dimensions [33]. Here, we envision an optical setting where two types of waveguides are used such that one of them is linear for the considered propagation. A recent example of such binary waveguides (yet in an alternating fashion so as to form a periodic linear-nonlinear waveguide array) appears e.g. in [34], where narrower waveguides are highly nonlinear whereas wider ones are almost linear. It is, however, straightforward to mold the relevant geometry of these ribs (appearing e.g. in Fig. 1 of [34]) in order to construct the lattice of interest herein. Then, the gain and loss can additionally be imparted to the lattice according to the prescription of [5].

Our presentation is structured as follows. In section II, we will give an overview of the relevant theory (some of the pertinent, details are relegated to an appendix). In section III, the analytical results are illustrated through numerical computations of both the transmittivities and rectification factors (both for the plane wave structures and for the Gaussian wavepackets) and of the existence, spectral stability and nonlinear dynamics of the plane waves. Finally, in section IV, we summarize our findings and present some directions for future studies.

## THEORETICAL ANALYSIS

### Stationary DNLS

Starting our considerations with the existence of stationary solutions of the infinite chain of interest, we examine the set of algebraic equations

$$\omega\psi_n = V_n\psi_n - \psi_{n+1} - \psi_{n-1} + \alpha_n|\psi_n|^2\psi_n \quad (1)$$

on a one-dimensional lattice for  $\psi_n \in \mathbb{C}$  and  $\omega \in \mathbb{R}$ . The parameters  $V_n \in \mathbb{C}$  and  $\alpha_n \in \mathbb{R}$  are zero everywhere except for  $1 \leq n \leq N$  so that the wave propagates freely outside of a finite region containing the nonlinearity and the (intended to be PT-symmetric, hence generally complex) linear potential. Rearranging (1) one obtains the so-called backward transfer map

$$\psi_{n-1} = -\psi_{n+1} + (V_n - \omega + \alpha_n|\psi_n|^2)\psi_n \quad (2)$$

from which solutions to (1) can be constructed from knowledge of  $\psi_n$  at two nodes.

The class of solutions whose (transmission and reflection) properties will be theoretically analyzed consists of plane waves of the form

$$\psi_n = \begin{cases} R_0 e^{ik_0 n} + R e^{-ik_0 n} & n \leq 1 \\ T e^{ik_0 n} & n \geq N \end{cases} \quad (3)$$

with  $R_0, R, T \in \mathbb{C}$  representing the incident, reflected and transmitted amplitudes, respectively and  $k_0 \geq 0$  is the wavenumber. Note that outside of the nonlinear region, for  $n < 1$  and  $n > N$ , (3) satisfies (1) for any  $R_0, R$  and  $T$  if  $\omega = -2 \cos(k_0)$ . Also directly from (3) [as applied to sites with  $n = 0$  and  $n = 1$ ], we have

$$R_0 = \frac{e^{-ik_0}\psi_0 - \psi_1}{e^{-ik_0} - e^{ik_0}} \quad \text{and} \quad R = \frac{e^{ik_0}\psi_0 - \psi_1}{e^{ik_0} - e^{-ik_0}}. \quad (4)$$

Thus, for any fixed values of  $k_0$  and  $T$ ,  $\psi_0$  and  $\psi_1$  can be calculated by applying (2) iteratively starting with  $\psi_N = Te^{ik_0N}$  and  $\psi_{N+1} = Te^{ik_0(N+1)}$  from (3). Then, (4) gives the appropriate values of  $R_0$  and  $R$  so that (1) is satisfied at all nodes. Such a procedure of finding the input as a function of the output (sometimes referred to as a ‘‘fixed output problem’’ [35]) is necessary to deal with the multistability which is often found for nonlinear problems, including our case (at least for a subset of parameters).

For convenience we write the backward transfer map with  $n = N - l + 1$  and in terms of  $\Psi_n$  for  $\psi_n \stackrel{def.}{=} Te^{ik_0N}\Psi_n$ . This gives for our infinite lattice:

$$\Psi_{N-l} = -\Psi_{N-l+2} + \delta_{N-l+1}\Psi_{N-l+1} \quad (5)$$

for  $\delta_j \stackrel{def.}{=} V_j - \omega + \alpha_j|T|^2|\Psi_j|^2$ . For example, applying (5) with  $N = 2$  and  $\Psi_3 = e^{ik_0}$ ,  $\Psi_2 = 1$  gives

$$\begin{aligned} \delta_2 &= V_2 - \omega + \alpha_2|T|^2 \\ \Psi_1 &= -e^{ik_0} + \delta_2 \\ \delta_1 &= V_1 - \omega + \alpha_1|T|^2|\delta_2 - e^{ik_0}|^2 \\ \Psi_0 &= -1 + \delta_1(\delta_2 - e^{ik_0}). \end{aligned} \quad (6)$$

Finally by (4) and (6) we have

$$R_0 = \frac{Te^{ik_0}}{e^{-ik_0} - e^{ik_0}} (-1 + (\delta_1 - e^{ik_0})(\delta_2 - e^{ik_0})) \quad (7)$$

and the corresponding transmission coefficient  $t \stackrel{def.}{=} |T|^2/|R_0|^2$  is then

$$t = \left| \frac{e^{ik_0} - e^{-ik_0}}{1 + (\delta_1 - e^{ik_0})(e^{ik_0} - \delta_2)} \right|^2. \quad (8)$$

In the linear case ( $\alpha_1 = \alpha_2 = 0$ ), it is immediately seen that  $t$  is the same for waves coming from the left or right side, independently of  $V_n$ , as prescribed by the reciprocity theorem. For a more detailed discussion of the linear case see e.g. Ref. [37].

It should be noted here that although the relevant calculation was presented for  $N = 2$ , it can be performed for arbitrary values of  $N$  (naturally, the complexity of the intermediate steps is increased, the higher the value of  $N$ ). Some of the relevant details for larger  $N$  have been provided in the Appendix. We should also note that in comparison to the earlier work of [29], there are fundamental similarities in the approach but also important differences in the nature of the results since our quantities  $\delta_i$  (corresponding to the  $\nu$  and  $\delta$ , respectively in [29]) are now, in principle, complex rather than purely real. Let us also indicate here that to quantify asymmetric propagation we will use the definition of a rectification factor  $f$  in the form:

$$f = \frac{t(k_0, T) - t(-k_0, T)}{t(k_0, T) + t(-k_0, T)}, \quad (9)$$

where we adopt the convention that  $-k_0$  denotes right-incoming solutions with wavenumber  $k_0$ . Non-vanishing values of  $f$  in the range  $[-1, 1]$  are measures of the asymmetry of transmission in the system (symmetric transmission is tantamount to  $f = 0$ ).

### Time Propagation

We also briefly touch upon the tools that we will use towards the consideration of the dynamical evolution phenomena within our nonlinear Schrödinger type chains

$$i\dot{\phi}_n(t) - V_n\phi_n(t) + \phi_{n+1}(t) + \phi_{n-1}(t) = \alpha_n|\phi_n(t)|^2\phi_n(t). \quad (10)$$

In particular, in addition to direct numerical integration of Eq. (10), so as to monitor the dynamical evolution of the solutions, we will use a spectral stability analysis of stationary states (of the form  $\psi_n e^{-i\omega t}$  discussed in the previous section) according to

$$\phi_n(t) = \rho_n(t) + \epsilon p_n(t). \quad (11)$$

Here,  $\rho_n(t) = \psi_n e^{-i\omega t}$  and  $p_n(t) = e^{-i\omega t} (a_n e^{i\nu t} + b_n e^{-i\nu^* t})$  for  $\omega \in \mathbb{R}$  and  $a_n, b_n, \nu \in \mathbb{C}$ .  $\rho_n$  is assumed to be a standing wave solution of (10) so that the resulting order- $\epsilon$  equation for  $p_n(t)$  is

$$i\dot{p}_n - V_n p_n + p_{n+1} + p_{n-1} + \omega p_n = \alpha_n (2p_n |\rho_n|^2 + \rho_n^2 p_n^*). \quad (12)$$

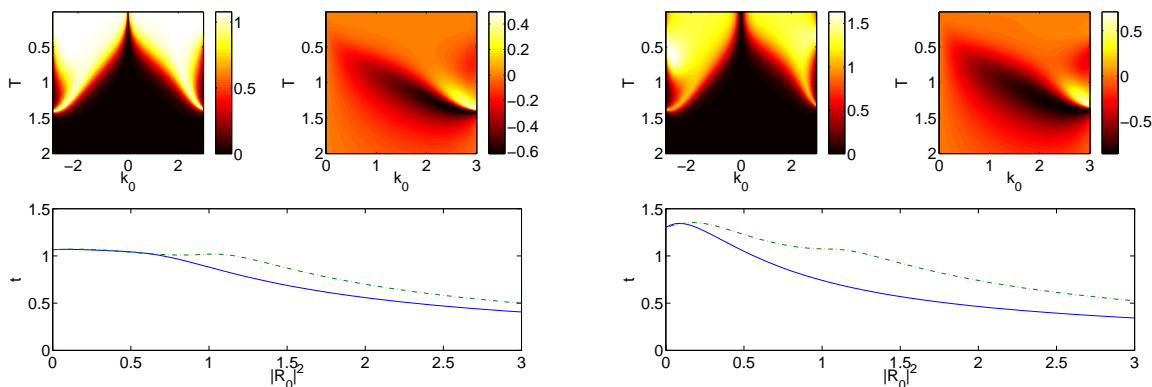


FIG. 1: The figure presents the case of a PT-symmetric dimer with  $N = 2$ ,  $\alpha_{1,2} = 1$ , while  $V_1 = i\gamma$  and  $V_2 = -i\gamma$ . The left set of panels corresponds to the case of  $\gamma = 0.25$ , while the right set of panels corresponds to the case of  $\gamma = 0.5$ . Each set contains a contour plot of  $t(k_0, T)$  (top left), a contour plot of  $f(k_0, T)$  (top right) and a typical example of the dependence of  $t$  for  $k_0 = 2$  (solid lines) and  $k_0 = -2$  (dashed lines), so as to illustrate the asymmetry between the propagation for left and right incident waves (bottom panels). In the latter the dependence of  $t$  is given as a function of  $|R_0|^2$ .

The ensuing linear stability equations will yield the eigen-problem of the form:

$$\nu \begin{pmatrix} a_n \\ b_n^* \end{pmatrix} = \begin{pmatrix} F_1 & F_2 \\ F_3 & F_4 \end{pmatrix} \begin{pmatrix} a_n \\ b_n^* \end{pmatrix} \quad (13)$$

for

$$\begin{aligned} F_1 &= \text{diag}(\omega - V_n - 2\alpha_n |\psi_n|^2) + G \\ F_2 &= \text{diag}(-\alpha_n \psi_n^2) \\ F_3 &= \text{diag}(\alpha_n (\psi_n^*)^2) \\ F_4 &= \text{diag}(-\omega + V_n^* + 2\alpha_n |\psi_n|^2) - G, \end{aligned} \quad (14)$$

where  $G$  is a sparse matrix with ones on the superdiagonal and the subdiagonal. Note that in (13) it is now convenient to think of  $a_n$  and  $b_n$  as column vectors. Given a stationary solution  $\rho_n$  and values of  $V_n, \alpha_n$  which encode the nonlinearity for  $1 \leq n \leq N$ , one then calculates the eigenvalues  $\nu$  in (13). If  $\nu$  has a negative imaginary part this indicates that the perturbed solution  $\phi_n(t)$  is unstable, as is easily seen by the form of  $p_n(t)$  specified above. In practice, one diagonalizes a finite truncation of the matrix in (13), ensuring that the relevant eigenvalues are not affected by the truncation error.

## NUMERICAL COMPUTATIONS

We now turn to computations in order to quantify the above theoretical results (as well as to extend beyond the range of what is analytically tractable).

We start with the consideration of the transmittivity  $t(k_0, T)$  and of the rectification factor  $f(k_0, T)$  which are given for the case of the PT-symmetric dimer in Fig. 1 and for the PT-symmetric trimer in Fig. 2. The nonlinearity is uniform in both cases, but the linear potential is  $V_1 = -V_2 = i\gamma$  in the former, while it is  $V_1 = -V_3 = i\gamma$  and  $V_2 = 0$  in the latter. In both cases, a typical example of the transmittivity dependence for  $k_0 = 2$  and  $k_0 = -2$  is shown in the bottom panels of the figures. The asymmetry which is present in the top left panels between positive and negative values of  $k_0$  and which is further quantified in the rectification factor of the top right panels clearly makes the case for the asymmetric wave propagation in these PT-symmetric oligomers. Although the values used here are below the PT transition of the underlying linear oligomer system, we have ensured that the relevant characteristic behavior (and presented asymmetries) exist both below and above that transition. However, as can also be inferred from the figures, the higher the value of PT-symmetric parameter  $\gamma$ , the stronger the manifestations of the asymmetric propagation of the waves. Another relevant observation to make here is that although the rectification factor is by construction bounded within  $[-1, 1]$ , the transmittivity is not bounded by unity (contrary to what is the case in the Hamiltonian example of [29]). Hence, we can observe that in all the examples of  $t$  shown the relevant factor may exceed unity thus illustrating the existence of gain in the system. It should be also noted that the rectification mechanism considered in Ref. [29] relies on multistability and resonance shifts. A remarkable difference here is that

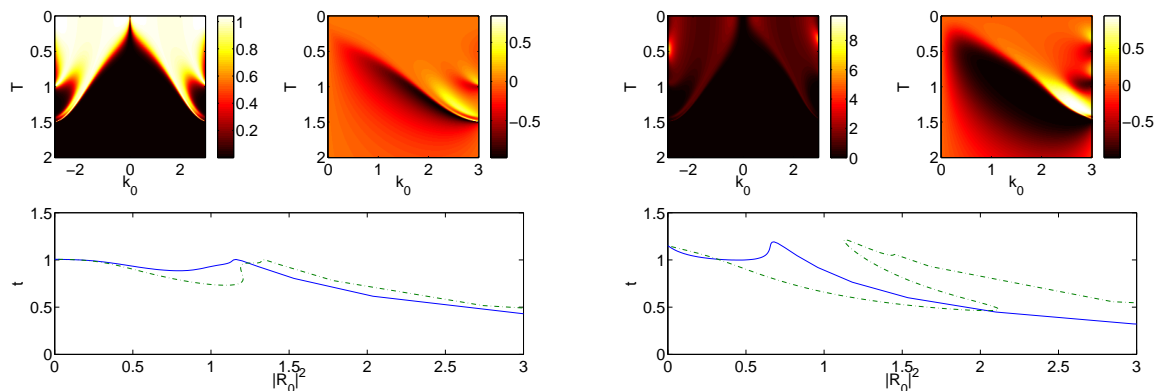


FIG. 2: Same as the figure above but now for the trimer case of  $N = 3$ ,  $\alpha_{1,2,3} = 1$ , while  $V_1 = i\gamma$ ,  $V_2 = 0$  and  $V_3 = -i\gamma$ . The specific values of  $\gamma$  for the panels given are  $\gamma = 0.1$  and  $\gamma = 0.45$ .

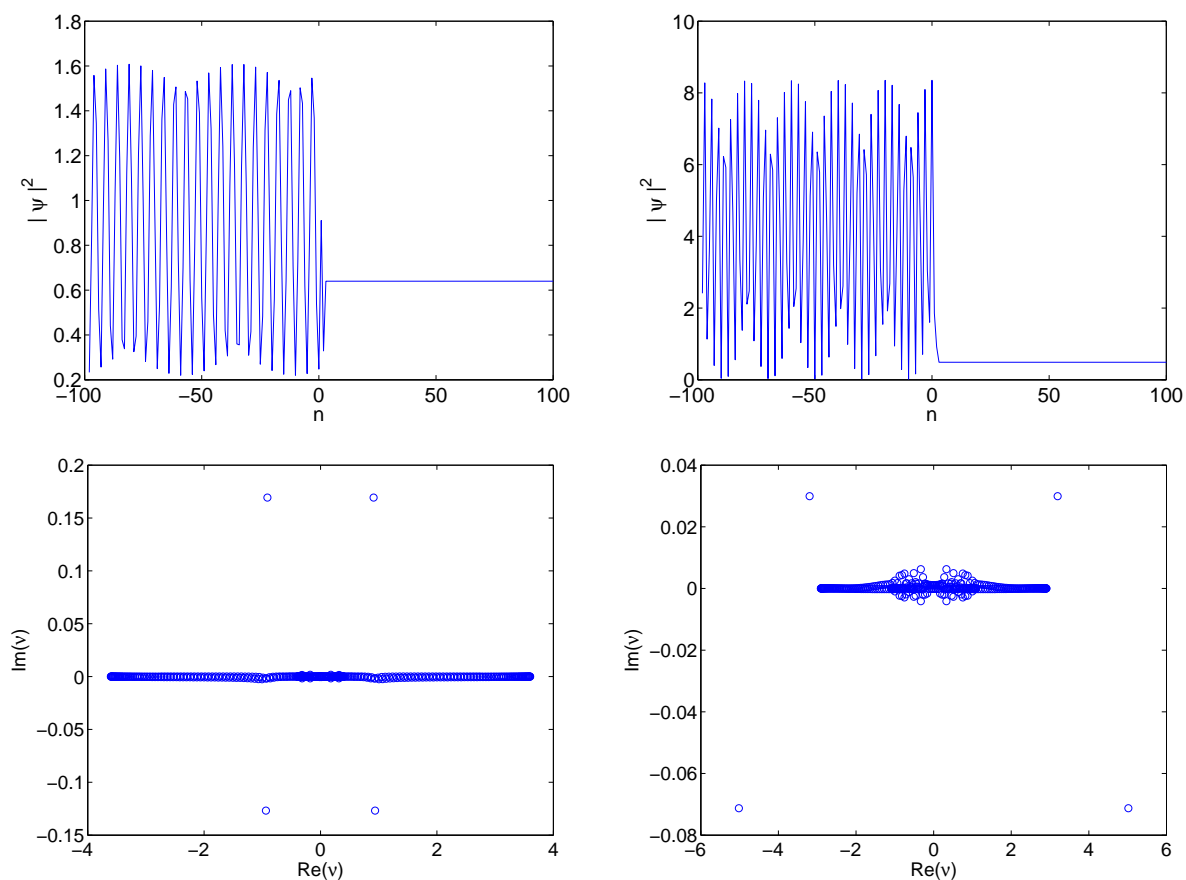


FIG. 3: The bottom panels show eigenvalues of the linearization of the example solutions shown in the top panel. In the PT-symmetric dimer (left), the parameters are  $N = 2$  with  $k_0 = 2.5$ ,  $T = 0.8$ ,  $\gamma = 0.1$ , while in the PT-symmetric trimer (right), they are:  $N = 3$  with  $k_0 = 1.1$ ,  $T = 0.7$ ,  $\gamma = 0.1$ .

in the instances shown in Fig. 1 there is no multistability, i.e., the output is a single-valued function of the input. Despite this, the rectifying effect remains sizeable as  $|f|$  can be still pretty large. This can be attributed to the presence of gain in the systems that appears to enhance the transmission with respect to the Hamiltonian case. It should be noted that similar observations can be made for the trimer in the case of small  $\gamma$  (cf. left panel of Fig. 2). Yet for sufficiently large values of  $\gamma$  (cf. the right panel of Fig. 2) multistability arises and, in turn, contributes to the observed rectification.

We now wish to touch upon the problem of the stability of the extended solutions  $\psi_n$ , identified in the form of

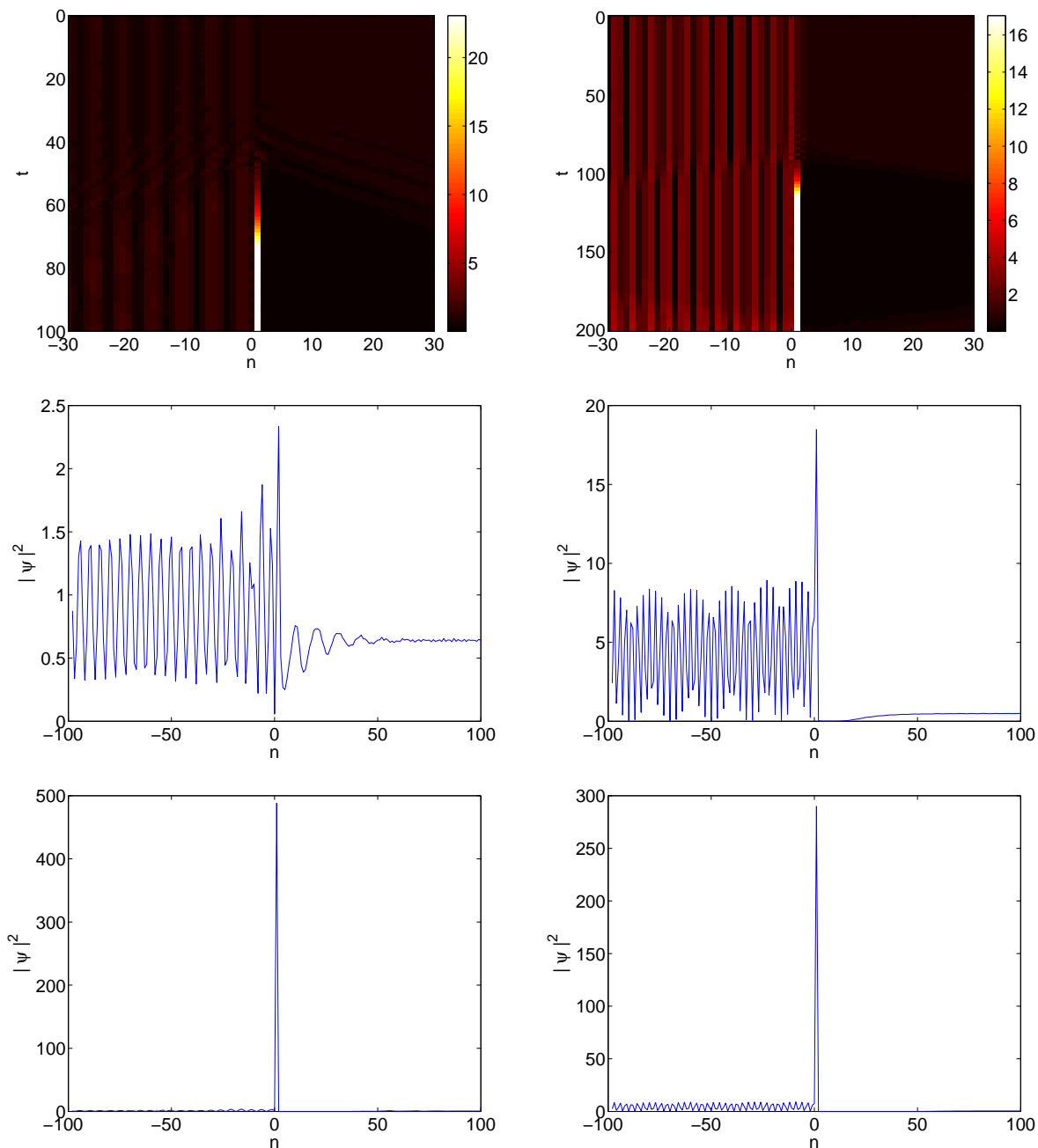


FIG. 4: The top panel shows the contour plot of the space  $n$  - time  $t$  evolution of  $|\phi_n|$  for the solutions/parameters corresponding to the left and right, respectively, panels of Fig. 3. The rest of the panels show individual snapshots of the solution at  $t = 50, 80$  (for the left panels of the dimer case) and at  $t = 100, 120$  (for the right panels of the trimer case).

Eq. (3). A complete stability analysis would require to take into account the fact that the lattice is infinite and that the eigemodes associated with the unstable eigenvalues (when they exist) are exponentially localized around the oligomers. To our knowledge an exhaustive study of this problem has not been reported in the literature (see e.g. Ref. [36] for a related study in the continuum case). A more complete analysis will be reported elsewhere. In the present work we limit ourselves to the illustration of a few representative cases. Typically, the relevant solutions are found to be unstable. An example of the corresponding spectral plane ( $\text{Re}(\nu), \text{Im}(\nu)$ ) of eigenfrequencies  $\nu = \text{Re}(\nu) + i \text{Im}(\nu)$  is shown for the case of the dimer and a corresponding one of the trimer in Fig. 3. In fact, our computations indicate that this feature persists in the Hamiltonian variant of the model of Ref. [29] (although a more detailed examination of the latter is of interest in its own right). The dynamical instability observed via the presence of imaginary eigenfrequencies in the spectral plane of the PT-symmetric oligomers is corroborated by direct numerical simulations in Fig. 4. Here, we initialize the lattice with the solutions that were shown to be unstable via the spectral analysis of Fig. 3, to which a normally distributed small amplitude random perturbation has been superposed. The

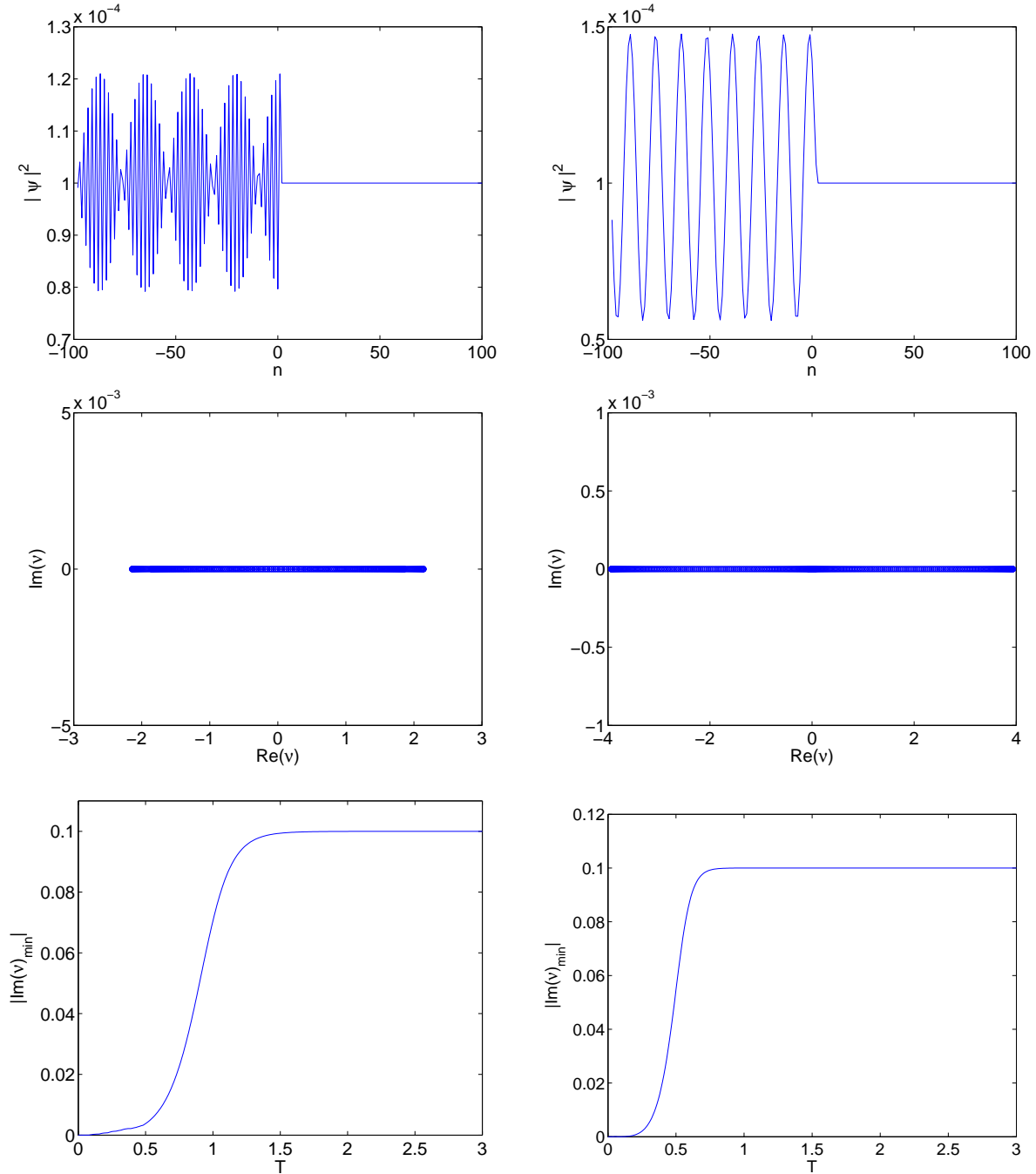


FIG. 5: The top panels show the dimer and trimer solution profiles for a small value of  $T = 0.01$  (and  $k_0 = 1.5$ ,  $\gamma = 0.1$  for the dimer, while  $k_0 = 0.25$ ,  $\gamma = 0.1$  for the trimer). The middle panels show the corresponding linear stability eigenfrequencies for this near-linear, stable case. Finally, the bottom panels show the dependence of the maximal growth rate (maximal negative imaginary eigenfrequency) as a function of the transmission parameter  $T$  of the wave, showing the significant instability enhancement upon progressive departure from the linear limit of  $T \rightarrow 0$ .

manifestation of the instability once again clearly underscores the role of the gain in the system. In particular, the dynamics reveals the tendency of the site which has gain to acquire a super-critical “mass” (or density), which subsequently grows exponentially well beyond the density of the linear background (or of the sites with loss).

A natural question about these extended states concerns the dependence of the instability on the strength of the nonlinearity. We explore this issue now by means of the results shown in Fig. 5. In particular, we vary the value of the transmitted amplitude  $T$  in order to systematically approach the linear limit which corresponds to  $T \rightarrow 0$ . For small  $T$ , the overall amplitude of the solution is small and the nonlinearity within the problem becomes negligible, giving essentially rise to linear states. For such sufficiently small values of  $T$ , the growth rate of the relevant instability is found to be negligible. We have given an example in the figure of such a small  $T$ , stable waveform and its linear

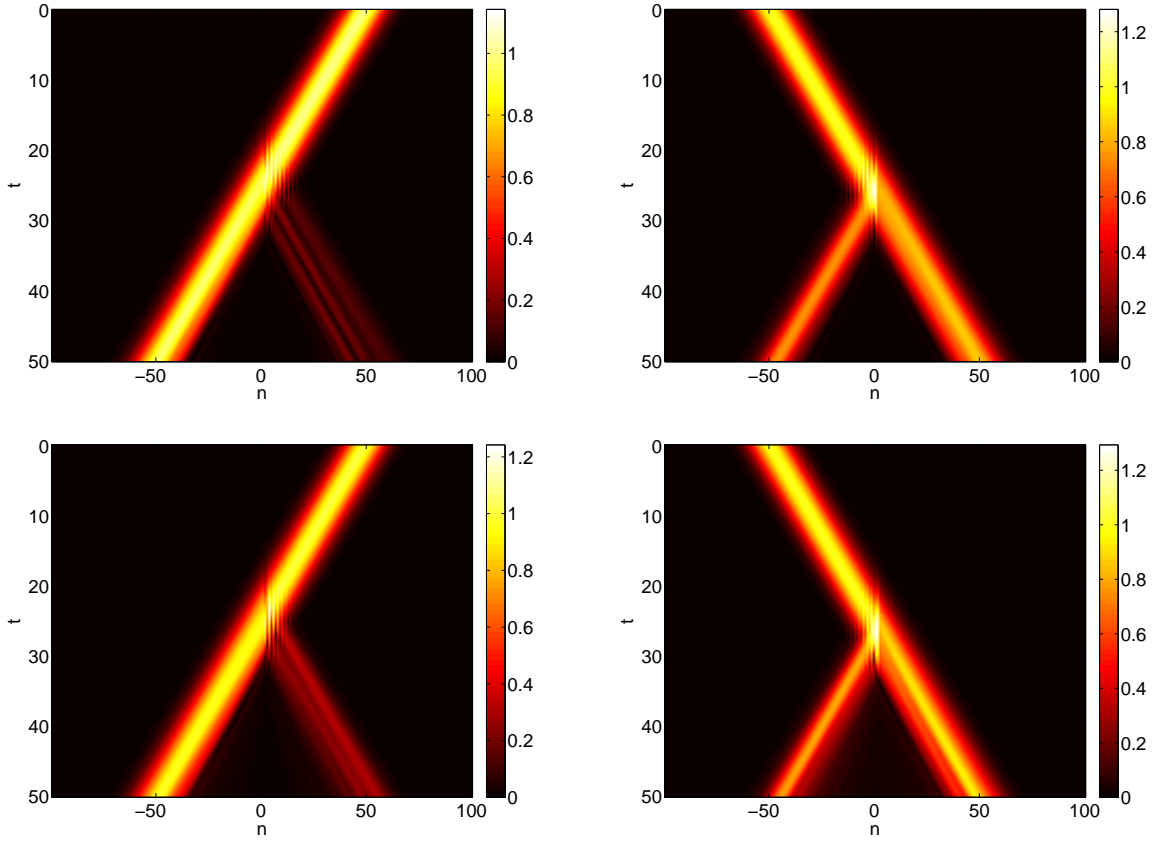


FIG. 6: The space-time contour plot of  $|\phi_n(t)|^2$  is shown for left and right incidence on the PT-symmetric dimer (top panels) and on the PT-symmetric trimer (bottom panels). Top: dimer,  $N = 2$  with  $n_0 = -50$ ,  $s = 10$ ,  $k_0 = -\pi/2$  (left) and  $k_0 = \pi/2$  (right); Bottom: trimer,  $N = 3$  with  $n_0 = -50$ ,  $s = 10$ ,  $k_0 = -\pi/2$  (left) and  $k_0 = \pi/2$  (right),

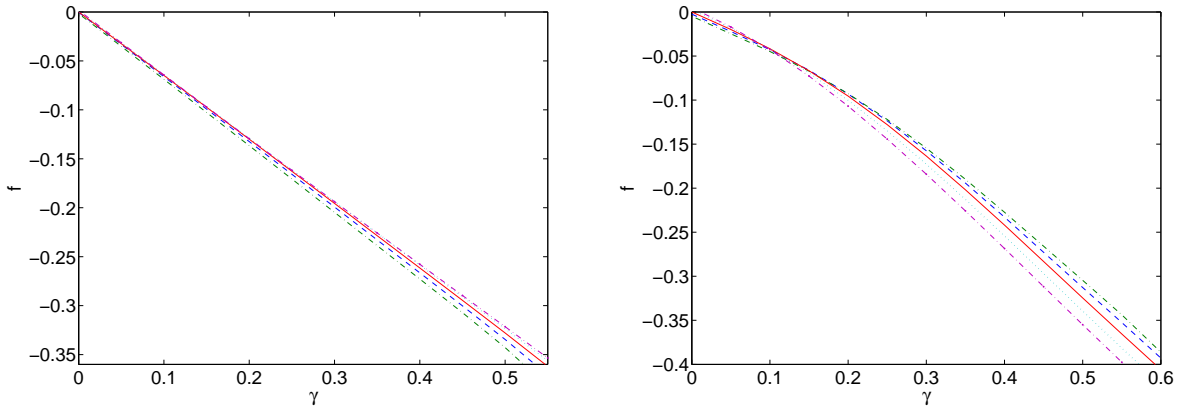


FIG. 7: Rectifying factor for the incidence of a Gaussian wavepacket on the PT-symmetric dimer and trimer. Left: dimer,  $N = 2$  with  $\alpha_1 = 1 - \Delta\alpha/2$ ,  $\alpha_2 = 1 + \Delta\alpha/2$  and  $k_0 = \pi/2$ ,  $n_0 = -50$ ,  $s = 10$ ; Right: trimer,  $N = 3$  with  $\alpha_1 = 1 - \Delta\alpha/2$ ,  $\alpha_2 = 1$ ,  $\alpha_3 = 1 + \Delta\alpha/2$  and  $k_0 = \pi/2$ ,  $n_0 = -50$ ,  $s = 10$ . The following values of  $\Delta\alpha$  are plotted:  $-0.5$  (dashed lines),  $-0.25$  (dashed-dotted),  $0$  (solid),  $0.25$  (dotted),  $0.5$  (dashed with bold dots).

stability analysis, and also show the dependence of the growth rate of the instability through the largest negative imaginary eigenfrequency as a function of  $T$  both for the dimer and the trimer. The latter clearly illustrates how the instability strength grows as a function of the nonlinearity. For both the dimer and the trimer solutions instability arises roughly at  $T \approx 0.25$ , as we see in the bottom panel of Fig. 5.

Given the above considerations and also the lesser physical relevance of exciting an initial condition of the form of Eq. (3) in an optical setting (which would be the prototypical potential realization of the considerations presented



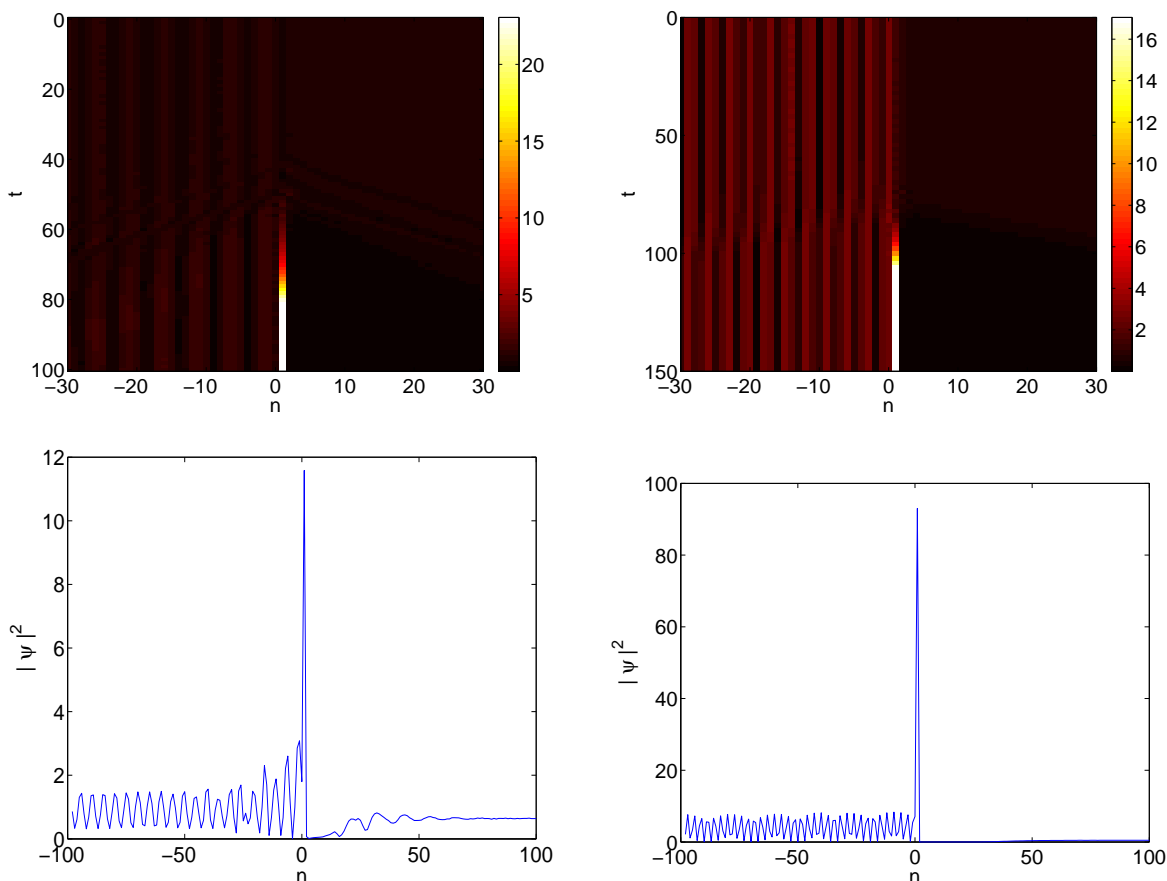


FIG. 8: This figure is a non-PT-symmetric analogue of Fig. 4. The top panel shows the contour plot of the space  $n$  - time  $t$  evolution of  $|\phi_n|$  for the dimer (left) with  $V_1 = 0.1i$ ,  $V_2 = -0.09i$  and  $k_0 = 2.5$ ,  $T = 0.8$ . The trimer (right) panels have parameters  $k_0 = 1.1$ ,  $T = 0.7$  with  $V_1 = 0.1i$ ,  $V_2 = 0$ ,  $V_3 = -0.09i$ . The bottom panels show individual snapshots of the solution at  $t = 50$  for the dimer and at  $t = 100$  for the trimer.

herein), we now turn to the examination of the dynamics of a more localized Gaussian wavepacket. The latter is assumed to be of the form:

$$\psi_n(0) = I e^{ik_0 n - (n-n_0)^2/s^2}, \quad (15)$$

i.e., of amplitude  $I$ , centered at  $n_0 \in \mathbb{Z}$ , while its speed is controlled by the parameter  $k_0$  ( $k_0 > 0, n_0 < 0$  for left-incoming packets and  $k_0 < 0, n_0 > N$  for right-incoming ones). The value of  $s$  (chosen to assume the value 10 in what follows) determines the wavepacket width. To minimize the dispersive effects and thus render negligible the dependence of the scattering process on the initial position  $n_0$ , we limited ourselves to the case in which  $|k_0| = \pi/2$ . It should, however, be noted that for different values of  $k_0$  (and especially for ones significantly deviating from the above band center), the dispersive nature of the discrete medium would make the results dependent not only on  $k_0$  but also  $n_0$ . It should be noted here that this aspect of our consideration is purely numerical (as it is not straightforward to obtain explicit analytical expressions for the transmission and reflection coefficients in this case). For a nonlinear system, there is no straightforward correspondence between the transmission coefficients of plane waves and the one of a wavepacket (in the language of Ref. [35] the latter it is a fixed input problem). Nevertheless, arguably, both problems are of interest. The fixed output problem examined above can be analytically studied and features such as bistability or asymmetric transmittivity can be quantified. Yet in the fixed input problem considered below some of these features (such as the asymmetric transmittivity) can be measured in ways that are conducive towards experimental realizations. We thus evolve an incident wavepacket from the left or from the right and observe its propagation as illustrated in the space-time contour plots of Fig. 6. In what is shown below, we have performed the numerical computations for  $I = 1$ , but we have confirmed that the relevant phenomenology persists for a wide range of non-vanishing values of  $I$  (approaching the linear limit of  $I \rightarrow 0$  leads to vanishing transmittivity differences, once again due to the principle of reciprocity).

The transmission coefficient in this case is defined as the fraction of the total sum of the squared modulus of the field across nodes that is transmitted to the right of the PT-symmetric oligomer after the Gaussian wavepacket passes

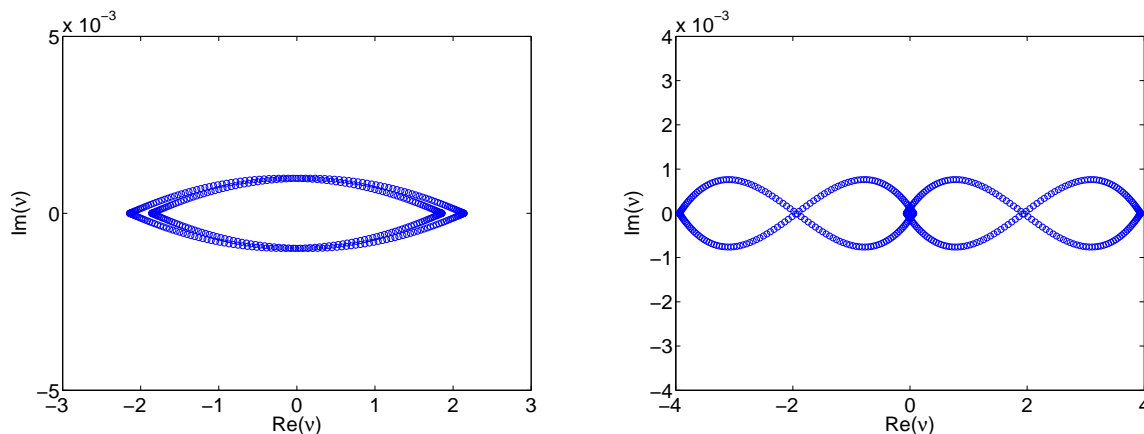


FIG. 9: This figure is the an analogue of Fig. 5 but with an asymmetric lattice adding one extra linear node to the right-hand-side of the chain. The panels show the eigenfrequencies for this now unstable case with the same small value of  $T = 0.01$  (again  $k_0 = 1.5, \gamma = 0.1$  for the dimer on the left and  $k_0 = 0.25, \gamma = 0.1$  for the trimer on the right).

over the relevant nodes. That is, we define  $t_{k_0} = \sum_{n < 1} |\phi_n|^2 / \sum_n |\phi_n|^2$  for  $k_0 < 0$  and  $t_{k_0} = \sum_{n > N} |\phi_n|^2 / \sum_n |\phi_n|^2$  for  $k_0 > 0$ . We find that the transmittivity is greater for Gaussians approaching from the right and that the transmittivity difference is amplified as  $\gamma$  increases, see Fig. 7 which presents the relevant rectifying factor. This can be qualitatively understood once again on the basis of the structure of the PT oligomer. The node that has gain (which is on the left) favors reflection for a wavepacket from the left, while it favors transmission for a wavepacket impinging from the right, hence ensuring that  $t_{-k_0} > t_{k_0}$  in our setup. Interestingly, in this case of the Gaussian wavepacket as well, for a high enough value of  $\gamma$  the density accumulates and grows indefinitely at the nonlinear node that bears the gain. On the dimer with  $\alpha_1 = \alpha_2 = 1$  we find that for  $k_0 = \pi/2$  this critical value is  $\gamma \simeq 0.6531$ , and for  $k_0 = -\pi/2$  it is  $\gamma \simeq 1.0890$ . On the trimer with  $\alpha_1 = \alpha_2 = \alpha_3 = 1$   $k_0 = \pi/2$  the blowup occurs for  $\gamma \simeq 0.6737$  and with  $k_0 = -\pi/2$  the value is  $\gamma \simeq 0.8043$ . We note once again that these features are unique to the case of PT-symmetric oligomers through their gain-loss pattern and would be entirely absent in the earlier Hamiltonian installment of such chains in [29]. This phenomenon can be seen as an illustration for the present system (and considered input wavepackets) of the phenomenology associated with the PT phase transition and its nonlinear analogs considered e.g. in works such as Refs. [7, 13] among others. What was found in the above systems (and is manifest here as well) is that past a critical value of gain-loss, the oligomer settings (and their lattice embedding generalization) are unable to balance the intended (through the gain-loss) growth and decay features through a gradient of the phase of the configuration. Instead, they become subject to indefinite growth (and corresponding decay in the lossy site). It should also be added here that Fig. 7 additionally contains the possibility of asymmetric nonlinearities (in the spirit of [29]), with the two sites bearing  $\alpha_1 = 1 - \Delta\alpha/2, \alpha_2 = 1 + \Delta\alpha/2$  and the three sites bearing  $\alpha_1 = 1 - \Delta\alpha/2, \alpha_2 = 1, \alpha_3 = 1 + \Delta\alpha/2$  for the dimer and trimer, respectively. It can be seen that the latter asymmetry provides a smooth change of the rectification factor with respect to the case  $\Delta\alpha = 0$ , which is more pronounced the higher the value of  $\Delta\alpha$ .

As a final comment, we revisit the comparison with the results of Ref. [29] and touch upon the specific role of the gain-loss balance within the PT-symmetric settings considered herein. As regards the former, and as alluded to previously, the broken parity symmetry is essential to the phenomenology reported herein and even to that of Ref. [29]. However, although in the latter the phenomenology was chiefly due to resonance shifts and creation of multi-stability, here it is far more so due to the existence of loss and gain. As we also illustrated in Fig. 7, by breaking the parity of the system within its nonlinear term, we may weakly affect the relevant phenomenology (or more strongly depending on the size of the parity breaking), yet the fundamental effects are still present and dominated by the loss-gain pattern.

Another deep question concerns the specific role of the gain-loss balance within our PT-symmetric system. In a sense, the exact pattern of gain-loss and its perfect balance is not that important for some aspects of the observed phenomenology. What is more important is that there be a parity breaking through the gain-loss pattern which will, in turn, induce the relevant transmission asymmetries and also features particular to our system (and not to the Hamiltonian variant of Ref. [29]) such as the indefinite growth and the transition to it beyond a certain gain strength. This is evident in Fig. 8 which showcases the instability induced growth for a case where the gain and loss coefficients are not perfectly balanced. To some extent, it should be added that something of this sort may be expected from past experience with variants of PT systems and their features, including e.g. the observation of the passive-PT phase transition [4], where the system only had two sites one without gain-loss and the other only

with loss. Nevertheless, it should be added that there *are* features of the system that critically (and quite subtly) may depend on whether the gain-loss pattern is perfectly balanced or not. We have accidentally bumped into a very simple and instructive example of this kind, when considering the effect of the lattice size. Consider a dimer embedded within the sites 100 and 101 of a lattice of size  $M = 200$ . Now, consider the same dimer within a lattice of size  $M = 201$ . It is straightforward to see that the former is perfectly PT-symmetric, while the latter is not (by what appears to be a negligible –far away– boundary contribution). Yet, if one considers the spectrum of the linear problem (and by extension the linearization spectrum of nonlinear states) within the two cases, one will *immediately* observe that the former system will be stable up to a finite critical point  $\gamma_{cr}$ , while the latter will become immediately (and nontrivially) unstable due to its violation of the exact PT symmetry – compare the spectra in Figs. 5 and 9. Moreover, the stronger and immediate instability implied by Fig. 9 has a bearing on the dynamics of the kind shown in Fig. 8 (cf. with the case of Fig. 4) given that the ensuing growth is manifested for earlier times in the case of asymmetric gain-loss. Hence, while certain aspects of the phenomenology (like the transmission asymmetry in the dynamics) may not be critically hinging on the perfect balance of gain and loss, others such as the stability of the nonlinear states (or the spectrum of the linear ones) upon introduction of gain and loss clearly do.

## CONCLUSIONS

In the present work, we considered a lattice setting where embedded in a linear Schrödinger chain was a nonlinear PT-symmetric oligomer, typically a dimer or a trimer. Our analytical considerations were focused around plane waves enabling us to analytically compute both the transmittivity and the rectification factor between left- and right-propagating such waves. These features amply evidenced the asymmetric nature of the propagation and even illustrated features particular to the gain-loss systems, such as the existence of over-unity transmittivities. On the other hand, we also considered the spectral stability of such states revealing their typical instability (except for the near-linear case) that was monitored and shown dynamically to lead to mass focusing on a single (gain) node of the lattice. This, in turn, led us to the consideration of the asymmetry of propagation of a Gaussian wavepacket which we numerically quantified. Here, too, however the interesting phenomenon of the potential trapping of mass in a particular site with gain and the subsequent indefinite growth thereof were observed and quantified. The effect of asymmetries in the nonlinearity and in the gain/loss profile were also examined.

These results suggest numerous interesting investigations for future work. It would be relevant to attempt to theoretically quantify transmittivities and reflectivities of a Gaussian wavepacket perhaps through a judicious variational ansatz or some similar method that appropriately reduces the degrees of freedom, while taking into consideration both the complex PT-oligomer dynamics and the generic existence of a reflecting and a transmitting wavepacket. On the other hand, it would be particularly interesting to generalize the relevant considerations to higher dimensional settings and examine how incident waves from different directions may affect the transmittivity of different forms of two-dimensional PT-symmetric oligomers (in the simplest genuinely two dimensional case, PT-symmetric squares [38]). These themes will be considered in future studies.

PGK gratefully acknowledges support from the US-NSF through grants DMS-0806762 and CMMI-1000337 and from the Alexander von Humboldt Foundation, the Alexander S. Onassis Public Benefit Foundation (through grant RZG 003/2010-2011) and from the Binational Science Foundation (through grant 2010239). SL acknowledges support from the Miur PRIN 2008 project *Efficienza delle macchine termoelettriche: un approccio microscopico*.

- 
- [1] C.M. Bender and S. Boettcher, Phys. Rev. Lett. **80**, 5243 (1998); C.M. Bender, S. Boettcher and P.N. Meisinger, J. Math. Phys. **40**, 2201 (1999)
  - [2] A. Ruschhaupt, F. Delgado, F. and J.G. Muga, J. Phys. A: Math. Gen., **38**, L171 (2005); A. Mostafazadeh and F. Loran, EPL, **81** 10007 (2008).
  - [3] Z.H. Musslimani, K.G. Makris, R. El-Ganainy and D.N. Christodoulides, Phys. Rev. Lett. **100**, 030402 (2008); K.G. Makris, R. El-Ganainy, D.N. Christodoulides and Z.H. Musslimani, Phys. Rev. A **81**, 063807 (2010).
  - [4] A. Guo, G. J. Salamo, D. Duchesne, R. Morandotti, M. Volatier-Ravat, V. Aimez, G. A. Siviloglou and D. N. Christodoulides, Phys. Rev. Lett. **103**, 093902 (2009).
  - [5] C.E. Rüter, K.G. Makris, R. El-Ganainy, D.N. Christodoulides, M. Segev, D. Kip, Nature Phys. **6**, 192 (2010).
  - [6] J. Schindler, A. Li, M.C. Zheng, F.M. Ellis and T. Kottos, Phys. Rev. A **84**, 040101 (2011).
  - [7] H. Ramezani, T. Kottos, R. El-Ganainy and D.N. Christodoulides, Phys. Rev. A **82**, 043803 (2010).
  - [8] A.A. Sukhorukov, Z. Xu and Yu.S. Kivshar, Phys. Rev. A **82**, 043818 (2010).
  - [9] M.C. Zheng, D.N. Christodoulides, R. Fleischmann and T. Kottos, Phys. Rev. A **82**, 010103(R) (2010).
  - [10] E.M. Graefe, H.J. Korsch and A.E. Niederle, Phys. Rev. Lett. **101**, 150408 (2008).
  - [11] E.M. Graefe, H.J. Korsch and A.E. Niederle, Phys. Rev. A **82**, 013629 (2010).
  - [12] Z. Lin, H. Ramezani, T. Eichelkraut, T. Kottos, H. Cao and D.N. Christodoulides, Phys. Rev. Lett. **106**, 213901 (2011).
  - [13] K. Li and P. G. Kevrekidis Phys. Rev. E **83**, 066608 (2011)

- [14] S.V. Dmitriev, S.V. Suchkov, A.A. Sukhorukov, and Yu.S. Kivshar, Phys. Rev. A **84**, 013833 (2011)
- [15] S.V. Suchkov, B.A. Malomed, S.V. Dmitriev and Yu.S. Kivshar, Phys. Rev. E **84**, 046609 (2011).
- [16] A.E. Miroshnichenko, B.A. Malomed, and Yu.S. Kivshar Phys. Rev. A **84**, 012123 (2011).
- [17] F.Kh. Abdullaev, Y.V. Kartashov, V.V. Konotop and D.A. Zezyulin, Phys. Rev. A **83**, 041805 (2011)
- [18] D. A. Zezyulin, Y. V. Kartashov, V. V. Konotop, arXiv:1111.0898.
- [19] Yu. A. Kosevich, Phys. Rev. B, **52**, 1017 (1995).
- [20] M. Terraneo, M. Peyrard, and G. Casati, Phys. Rev. Lett. **88**, 094302 (2002).
- [21] C.W. Chang, D. Okawa, A. Majumdar, and A. Zettl, Science **314**, 1121 (2006); W. Kobayashi, Y. Teraoka, and I. Terasaki, Appl. Phys. Lett. **95**, 171905 (2009).
- [22] M. Scalora, J. P. Dowling, C. M. Bowden, and M. J. Bloemer, J. Appl. Phys. **76**, 2023 (1994); M. D. Tocci, M. J. Bloemer, M. Scalora, J. P. Dowling, and C. M. Bowden, Appl. Phys. Lett. **66**, 2324 (1995).
- [23] V.V. Konotop and V. Kuzmiak, Phys. Rev. B **66**, 235208 (2002). B. Liang, B. Yuan and J.C. Cheng, Phys. Rev. Lett. **103**, 104301 (2009).
- [24] K. Gallo, G. Assanto, K. Parameswaran and M. Fejer, Appl. Phys. Lett. **79**, 314 (2001).
- [25] M.W. Feise, I.V. Shadrivov and Y.S. Kivshar, Phys. Rev. E **71**, 037602 (2005).
- [26] N. Boechler, G. Theocharis and C. Daraio, Nature Materials **10**, 665 (2011).
- [27] B. Liang, B. Yuan and J.C. Cheng, Phys. Rev. Lett. **103**, 104301 (2009); B. Liang, X.S. Guo, J. Tu, D. Zhang and J.C. Cheng, Nature Mater. **9**, 989992 (2010).
- [28] S. Longhi, J. Phys. A. **44**, 485302 (2011).
- [29] S. Lepri and G. Casati, Phys. Rev. Lett. **106**, 164101 (2011).
- [30] D. A. Zezyulin, V. V. Konotop, arXiv:1202.3652.
- [31] G.P. Tsironis, M.I. Molina and D. Hennig, Phys. Rev. E **50**, 2365 (1994).
- [32] M.I. Molina, H. Bahlouli Phys. Lett. A **284**, 87 (2002).
- [33] M. I. Molina Phys. Rev. B **60**, 2276 (1999).
- [34] K. Hizanidis, Y. Kominis and N.K. Efremidis, Opt. Express **16**, 18296 (2008).
- [35] R. Knapp, G. Papanicolaou and B. White, J. Stat. Phys. **63**, 567, (1991).
- [36] B. A. Malomed and M. Ya. Azbel. Phys. Rev. B, **47**, 10402–10406 (1993).
- [37] B.Lindquist, Phys. Rev. E **63**, 56605 (2001).
- [38] K. Li, P.G. Kevrekidis, B.A. Malomed, U. Guenther, arXiv:1204.5530.

## Appendix

For the record we show four iterations of (5) starting from  $\Psi_{N+1} = e^{ik}$  and  $\Psi_N = 1$ :

$$\begin{aligned}
\delta_N &= V_N - \omega + \alpha_N |T|^2 \\
\Psi_{N-1} &= -\Psi_{N+1} + \delta_N \Psi_N \quad (l=1) \\
&= -e^{ik} + \delta_N \\
\delta_{N-1} &= V_{N-1} - \omega + \alpha_{N-1} |T|^2 |\delta_N - e^{ik}|^2 \\
\Psi_{N-2} &= -\Psi_N + \delta_{N-1} \Psi_{N-1} \quad (l=2) \\
&= -1 + \delta_{N-1} (\delta_N - e^{ik}) \\
\delta_{N-2} &= V_{N-2} - \omega + \alpha_{N-2} |T|^2 |1 + \delta_{N-1} (e^{ik} - \delta_N)|^2 \\
\Psi_{N-3} &= -\Psi_{N-1} + \delta_{N-2} \Psi_{N-2} \quad (l=3) \\
&= e^{ik} - \delta_N + \delta_{N-2} (-1 + \delta_{N-1} (\delta_N - e^{ik})) \\
&= -\delta_{N-2} + (e^{ik} - \delta_N) (1 - \delta_{N-2} \delta_{N-1}) \\
\delta_{N-3} &= V_{N-3} - \omega + \alpha_{N-3} |T|^2 |\delta_{N-2} + (\delta_N - e^{ik}) (1 - \delta_{N-2} \delta_{N-1})|^2 \\
\Psi_{N-4} &= -\Psi_{N-2} + \delta_{N-3} \Psi_{N-3} \quad (l=4) \\
&= 1 + \delta_{N-1} (e^{ik} - \delta_N) + \delta_{N-3} (-\delta_{N-2} + (e^{ik} - \delta_N) (1 - \delta_{N-2} \delta_{N-1})) \\
&= 1 - \delta_{N-3} \delta_{N-2} + (e^{ik} - \delta_N) (\delta_{N-1} + \delta_{N-3} (1 - \delta_{N-2} \delta_{N-1})) \\
\delta_{N-4} &= V_{N-4} - \omega + \alpha_{N-4} |T|^2 |1 - \delta_{N-3} \delta_{N-2} + (e^{ik} - \delta_N) (\delta_{N-1} + \delta_{N-3} (1 - \delta_{N-2} \delta_{N-1}))|^2
\end{aligned}$$

Notice that if we iterate  $N$  times we get  $\delta$ 's equal to  $-\omega$  since  $V = \alpha = 0$  for these nodes. Then  $R_0$  can be calculated from (4) in terms of appropriate  $\delta$ 's.

For  $N = 3$ , the algorithm gives a transmission coefficient

$$t = \left| \frac{e^{ik} - e^{-ik}}{e^{ik} - \delta_1 + (e^{ik} - \delta_3)(1 - \delta_2(\delta_1 - e^{ik}))} \right|^2 \quad (16)$$

for

$$\begin{aligned}\delta_3 &= V_3 - \omega + \alpha_3 |T|^2 \\ \delta_2 &= V_2 - \omega + \alpha_2 |T|^2 |\delta_3 - e^{ik}|^2 \\ \delta_1 &= V_1 - \omega + \alpha_1 |T|^2 |1 + \delta_2 (e^{ik} - \delta_3)|^2.\end{aligned}\tag{17}$$

Similar results can be obtained for  $N = 4, 5, \dots$